

This is the accepted manuscript made available via CHORUS. The article has been published as:

Magnetic second-order topological insulators and semimetals

Motohiko Ezawa

Phys. Rev. B **97**, 155305 — Published 17 April 2018

DOI: [10.1103/PhysRevB.97.155305](https://doi.org/10.1103/PhysRevB.97.155305)

Magnetic second-order topological insulators and semimetals

Motohiko Ezawa

Department of Applied Physics, University of Tokyo, Hongo 7-3-1, 113-8656, Japan

We propose magnetic second-order topological insulators (SOTIs). First, we study a three-dimensional model. It is pointed out that the previously proposed topological hinge insulator has actually surface states along the [001] direction in addition to hinge states. We gap out these surface states by introducing magnetization, obtaining a SOTI only with hinge states. The bulk topological number is the Z_2 index protected by the combined symmetry of the four-fold rotation and the inversion symmetry. We next study two dimensional magnetic SOTIs, where the corner states are robust also in the presence of the magnetization. Finally, we construct a magnetic second-order topological semimetals by layering the two-dimensional magnetic SOTIs, where hinge-arc states are robust also in the presence of the magnetization.

Introduction: Topological insulators (TIs) have opened a new world in condensed matter physics^{1,2}. The first example is the quantum Hall insulator, where the topological number is the Chern number³. It is not necessary to require any symmetries for the quantization of the Chern number. The current movement of the topological insulator has started with the time-reversal invariant topological insulator^{4,5}, where the topological number is the Z_2 index protected by the time reversal symmetry (TRS). Then, it is generalized to the topological crystalline insulator, where the mirror Chern number is the topological number⁶. Here the mirror symmetry protects the topological phase. Recent interest is renewed in topological insulators protected by more general crystalline symmetries including the rotational symmetry⁷⁻¹².

Higher-order topological insulators are extension of the TIs¹³⁻²⁵, to which the conventional bulk-boundary correspondence is generalized. Here we focus on three dimensional (3D) crystals. Then, the second-order TI (SOTI) has 1D topological boundary states (hinge states) but has no 2D topological boundary states (surface states), while the third-order TI has 0D topological boundary states (corner states) but has neither surface states nor hinge states. Recently, bismuth was predicted and shown to be an SOTI theoretically and experimentally²⁶ by employing topological quantum chemistry²⁷⁻³². As a closely related concept to the SOTI, there are topological hinge insulators²⁰. They are TIs possessing topological hinge states. Note that they may have topological surface states in addition to hinge states. An example²⁰ was constructed by adding a nontrivial mass term to a 3D TI and by gapping out some topological surface states. Indeed, when we consider a cube parallel to the x , y and z axes in this example, there appear two surface states perpendicular to the z axis in addition to four hinge states: See Fig.1(b).

In this paper, introducing magnetization along the z axis, first we propose a 3D magnetic SOTI by gapping out all the surface states in the topological hinge insulator²⁰ just mentioned above. As we see in Fig.1(c) and (d), there appear only hinge states without surface states in the presence of the magnetization. The bulk topological number is shown to be the Z_2 index protected by the rotoinversion symmetry $\bar{C}_4 = C_4I$, which is the combined symmetry of the four-fold rotation C_4 and the inversion I . Second, we construct a 2D magnetic SOTI, where topological corner states appear. Finally, we construct a magnetic second-order topological semimetals

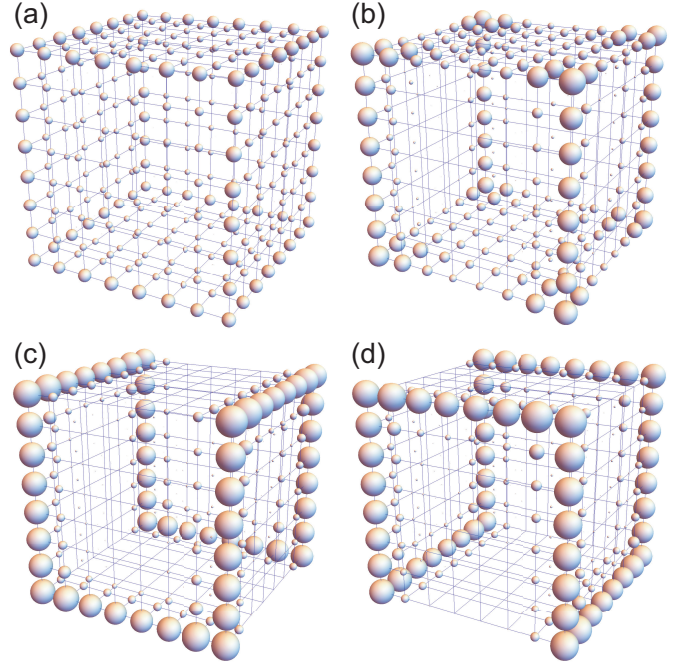


FIG. 1: 3D SOTI. The real-space plot of the square root of the local density of states $\sqrt{\rho_i}$ for a cube in the case of (a) the TI, (b) a topological hinge insulator, (c) and (d) magnetic SOTIs in the presence of magnetization with $B > 0$ and $B < 0$, respectively. The amplitude is represented by the radius of spheres. The size of the cube is $L = 8$. The local density of states becomes arbitrarily small for $L \gg 1$ except for (a) 6 surfaces, (b) 2 surfaces and 4 hinges, (c) and (d) for hinges.

based on the stacking of the 2D magnetic SOTI, where hinge-arc states emerge connecting the gap closing points.

3D magnetic SOTI: The typical model for the 3D TI is given by³³

$$H_0 = \left(m + t \sum_i \cos k_i \right) \tau_z \sigma_0 + \lambda \sum_i \sin k_i \tau_x \sigma_i \quad (1)$$

on the cubic lattice, where i runs over x, y, z . It describes³⁴ topological Kondo insulators SmB_6 . The σ_i represent the Pauli matrices corresponding to the spin degrees of freedom and σ_0 is the two by two identity matrix, while τ_i are the Pauli

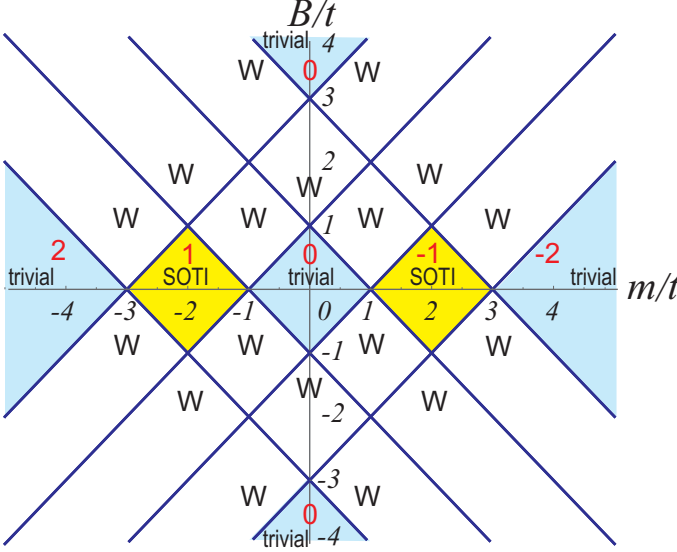


FIG. 2: 3D SOTI. Topological phase diagram in the $(m/t, B/t)$ plane. Numbers in red represent the Z index κ_4 , which gives the topological number ν by the formula $\nu = \text{mod}_2 \kappa_4$. The symbol W stands for Weyl semimetal phases. The SOTI phases are masked in yellow.

matrices corresponding to the orbital degrees of freedom. It has the TRS. Protected by the TRS, it has topological surface states in accord with the bulk-boundary correspondence as in Fig.1(a).

To gap out them by breaking the TRS, the following extra term has been proposed²⁰,

$$H_\Delta = \Delta (\cos k_x - \cos k_y) \tau_y \sigma_0. \quad (2)$$

Additionally we introduce the Zeeman term induced by magnetization,

$$H_Z = B \tau_0 \sigma_z. \quad (3)$$

We study the effect of the Zeeman term in the 3D topological hinge insulators in the following order.

Topological phase diagram: The band structure is obtained by diagonalizing the Hamiltonian $H = H_0 + H_\Delta + H_Z$. It follows that the phase boundaries are given by solving the zero-energy condition ($E = 0$) at the four high-symmetry points $\Gamma = (0, 0, 0)$, $S = (\pi, \pi, 0)$, $Z = (0, 0, \pi)$ and $R = (\pi, \pi, \pi)$ with respect to the four-fold rotation. The energies at these points are analytically given by

$$E(0, 0, 0) = 3t + m \pm B, \quad -3t - m \pm B, \quad (4)$$

$$E(\pi, \pi, 0) = t - m \pm B, \quad -t + m \pm B, \quad (5)$$

$$E(0, 0, \pi) = t + m \pm B, \quad -t - m \pm B, \quad (6)$$

$$E(\pi, \pi, \pi) = 3t - m \pm B, \quad -3t + m \pm B. \quad (7)$$

We show the phase diagram in Fig.2. In the absence of the Zeeman term²⁰, the system is topological for $1 < |m/t| < 3$ and trivial for $|m/t| < 1$ or $|m/t| > 3$: See Fig.2. Insulators emerge in the region including the phases with $B = 0$.

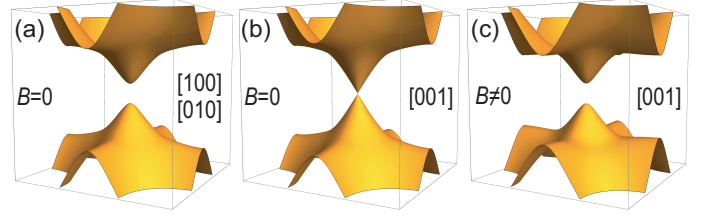


FIG. 3: 3D SOTI. Surface band structure of a thin film. Surface states of the topological hinge insulator. (a) along the $[100]$ and $[010]$ direction; (b) those along the $[001]$ direction, where the gap closes at the M point in the surface Brillouin zone; (c) Surface states of the magnetic SOTI along the $[001]$ direction with $B = t/2$. The surface states are gapped in the presence of magnetization.

Later we identify the bulk topological number ν and find that it changes its value at these phase boundaries: See (11). The phase diagram consists of topological and trivial insulator phases and Weyl semimetal phases.

Symmetries: In order to identify the bulk topological invariant, it is necessary to study the symmetry of the Hamiltonian H_0 . We note that $TH_0(\mathbf{k})T^{-1} = H_0(-\mathbf{k})$ and $IH_0(\mathbf{k})I^{-1} = H_0(-\mathbf{k})$, where $T = \tau_0 \sigma_y K$ generates the TRS with the complex conjugation K , while $I = \tau_z \sigma_0$ the inversion symmetry. In addition, there is a four-fold rotational symmetry C_4 ,

$$C_4 H_0(k_x, k_y, k_z) C_4^{-1} = H_0(-k_y, k_x, k_z), \quad (8)$$

where

$$C_4 = \tau_0 \exp \left[-\frac{i\pi}{4} \sigma_z \right] \quad (9)$$

is the generator of the $\pi/4$ rotation. The H_Δ breaks both of the TRS and the inversion symmetry but preserves²⁰ the combined symmetry $C_4 T$ and the rotoinversion symmetry $\bar{C}_4 = C_4 I$. Our concern is the effect of the Zeeman term. The Zeeman term H_Z breaks $C_4 T$ but preserves \bar{C}_4 .

Z_2 index protected by \bar{C}_4 : We can define^{12,20} the Z index κ_4 protected by the rotoinversion symmetry \bar{C}_4 ,

$$\kappa_4 = \frac{1}{2\sqrt{2}} \sum_K \sum_\alpha e^{\frac{i\alpha\pi}{4}} n_K^\alpha, \quad (10)$$

where K runs over the high symmetry points Γ, S, Z, R ; n_K^α is the number of the occupied bands with the eigenvalue $e^{\frac{i\alpha\pi}{4}}$ of the symmetry operator \bar{C}_4 , $\bar{C}_4|\psi\rangle = e^{\frac{i\alpha\pi}{4}}|\psi\rangle$. Because of the relation $(\bar{C}_4)^4 = -1$, α is quantized to be $\alpha = 1, 3, 5, 7$. We explicitly evaluate κ_4 using the formula (10), which is shown in Fig.2. It follows that the topological phases at $B = 0$ are extended to the regions with $B \neq 0$, as shown in Fig.2. When there is the TRS, there is a relation¹² that $\text{mod}_2 \kappa_4 = \nu_0$, where ν_0 is the Z_2 index for the time-reversal invariant topological insulators. Furthermore, by calculating the band structure of a square prism, we can check that no hinge states emerge for $B \neq 0$ in the phase indexed by $\kappa_4 = 0, \pm 2$ in the phase diagram (Fig.2). It implies that the bulk topological

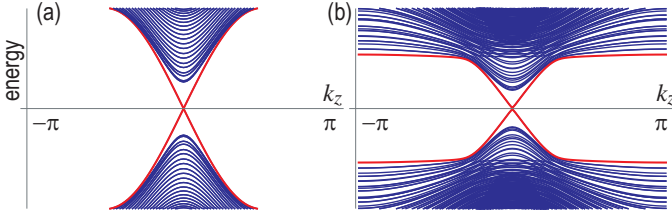


FIG. 4: 3D SOTI. Band structure of the hinge states (a) without the Zeeman term and (b) with the Zeeman term $B = t/2$. The hinge states survive even in the presence of the Zeeman term. The horizontal axis is the momentum k_z . We have set $m/t = 2$, $\lambda = t$ and $\Delta = t/4$.

index is given by

$$\nu = \text{mod}_2 \kappa_4, \quad (11)$$

which is a generalization of ν_0 in the absence of the TRS.

Surface states: We study the surface states in the topological phase. It is shown that the surface states along the [100] and [010] directions are gapped due to the term H_Δ as in Fig.3(a). However, we find the gapless surface states along the [001] direction as in Fig.3(b). This is because that the C_4T and \bar{C}_4 symmetries are preserved along the [001] direction but broken along the [100] and [010] directions. Because of the emergence of the topological surface states, the topological hinge insulator is not a SOTI. Nevertheless, this gapless surface states can be gapped out by introducing the Zeeman term as in Fig.3(c). On the other hand, the [100] and [010] surface states remain to be gapped in the presence of the Zeeman term.

Hinge states: We calculate the band structure of a square prism in the topological insulator phase to examine the hinge states. The hinge states remain as they are even in the presence of the magnetization, as shown in Fig.4. These hinge states are protected by the Z_2 index associated with the \bar{C}_4 symmetry.

2D magnetic SOTI: Next, we study a magnetic SOTI model in two dimensions. The Hamiltonian is given by setting $i = x, y$ in the Hamiltonian of the SOTI in three dimensions. The symmetry analysis is almost the same as in the 3D case just by neglecting the z coordinate. We discuss the properties of a 2D magnetic SOTI in the following order.

Topological phase diagram: The Brillouin zone is a square with four corners, $\Gamma = (0, 0)$, $X = (\pi, 0)$, $Y = (0, \pi)$ and $M = (\pi, \pi)$. The massive Dirac cone exists at the M point for $|m - 2t| < |m + 2t|$ and at the Γ point for $|m - 2t| > |m + 2t|$. There are two high-symmetry points, Γ and M . At these points the TRS and the C_4 symmetry are respected. The energy spectrum reads $E = \pm |2t + \eta m|$ with the two-fold degeneracy at the Γ point with $\eta = 1$ and at the M point with $\eta = -1$. In the presence of the Zeeman term, the energies at these points are analytically given by

$$E(0, 0) = 2t + m \pm B, \quad -2t - m \pm B, \quad (12)$$

$$E(\pi, \pi) = 2t - m \pm B, \quad -2t + m \pm B. \quad (13)$$

The topological phase diagram, given in Fig.5(a), consists of a SOTI phase, Chern TI (CI) phases and trivial insulator

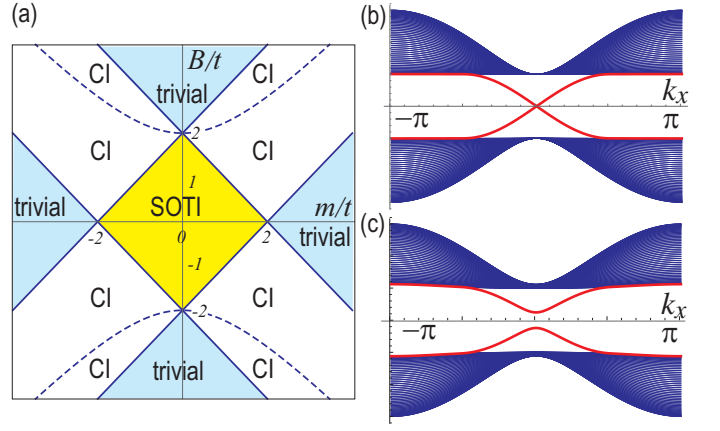


FIG. 5: 2D SOTI. (a) Topological phase diagram in the $(m/t, B/t)$ plane, which contains three distinctive phases: the trivial phase, the SOTI phase and the Chern TI (CI) phase. Band structures of (b) a nanoribbon in the absence of the H_Δ term and (c) the one in the presence of the H_Δ term, where we have chosen $\Delta = t/4$. Red curves represent edge modes in (b). We have set $m = \lambda = t$.

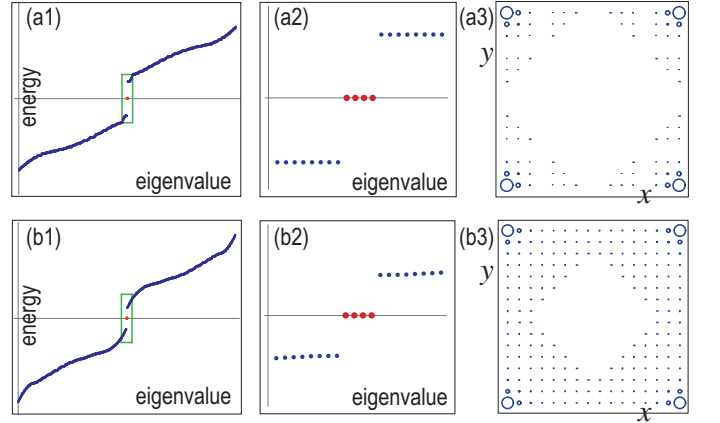


FIG. 6: 2D SOTI. Eigenvalues of the square (a) without magnetization and (b) with magnetization ($B = t/2$). (a2) and (b2) Enlarged figures of the green areas in (a1) and (b1). Four zero-energy states indicated in red are observed. (a3) and (b3) Corresponding local charge distributions. Charge distributions are well localized, where localization is slightly weakened in the presence of magnetization. We have set $m = \lambda = \Delta = t$.

phases. We can check there are chiral edge states for nanoribbons in the CI phase. We have also gap closing in the CI phase at $E(\pi, 0) = E(0, \pi) = 0$ with $E(\pi, 0) = E(0, \pi) = \sqrt{m^2 + 4\Delta^2} \pm B, -\sqrt{m^2 + 4\Delta^2} \pm B$, which are plotted in dotted curves in Fig.5(a).

Edge states: We calculate the band structure of nanoribbons without the Zeeman term in the topological phase ($|m/t| < 2$). In the absence of the H_Δ term, there are topological edge states as shown in Fig.5(b). They are gapped by the H_Δ term as shown in Fig.5(c). Namely, edge states are absent since the rotoinversion symmetry \bar{C}_4 is broken in the nanoribbon geometry.

Corner states: We calculate the eigenvalues of the Hamil-

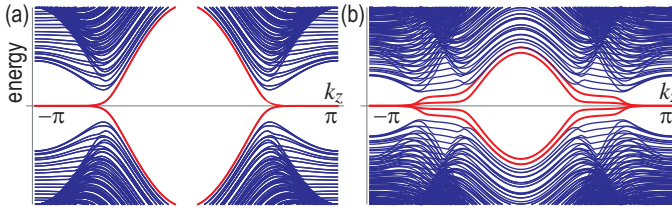


FIG. 7: 3D second-order topological semimetal. Band structure of hinge-arc states (a) without the Zeeman term and (b) with the Zeeman term ($B = t/2$). The hinge states survive even in the presence of the Zeeman term. The horizontal axis is the momentum k_z . We have set $m/t = 2$, $\lambda = t$ and $\Delta = t/4$.

tonian for a square nanodisk, which preserves the four-fold rotational symmetry. We show the eigenvalues in Fig.6(a1) and (a2) in the absence of the Zeeman term. There are four zero-energy states. These zero-energy states remain as they are even when the Zeeman term is introduced as in Fig.6(b1) and (b2). This is a 2D magnetic SOTI. We show the charge distribution in the absence and presence of the Zeeman term in Fig.6(a3) and (b3), respectively. The wave functions are localized at the four corners.

The origin of the gap opening in nanoribbon geometry and persistence of the corner states in the presence of the H_Δ term is naturally understood by treating the H_Δ as a perturbation²⁰.

The edge states at the zero energy is spatially uniform. The expectation value of the H_Δ term is Δ along the x direction while it is $-\Delta$ along the y direction. Thus, the edge states are gapped for a nanoribbon geometry. On the other hand, the expectation value of the H_Δ is exactly cancelled at the corner. As a result, the corner states are robust in the presence of H_Δ term.

3D second-order topological semimetals: By setting $m = m_0 + t_z \cos k_z$ in the 2D magnetic SOTI Hamiltonian, we can construct a model for 3D magnetic second-order topological semimetals in the similar way to the previous works^{22,35}. The properties are derived by the sliced Hamiltonian $H(k_z)$ along the k_z axis, which gives a 2D magnetic SOTI model with various mass term m . The bulk band gap closes at the points $k_z = \arccos[(m - m_0)/t_z]$. The surface states are gapped except for the two bulk gap closing points. On the other hand, there emerge hinge-arc states connecting the two gap closing points, which are shown in Fig.7(a). This hinge-arc states are robust even in the presence of the Zeeman term as shown in Fig.7(b).

The author is very much grateful to N. Nagaosa for helpful discussions on the subject. This work is supported by the Grants-in-Aid for Scientific Research from MEXT KAKENHI (Grant Nos.JP17K05490 and JP15H05854). This work is also supported by CREST, JST (JPMJCR16F1).

- ¹ M. Z. Hasan and C. L. Kane, Rev. Mod. Phys. **82**, 3045 (2010).
- ² X.-L. Qi and S.-C. Zhang, Rev. Mod. Phys. **83**, 1057 (2011).
- ³ D.J. Thouless, M. Kohmoto, M.P. Nightingale, M. den Nijs, Phys. Rev. Lett. **49** 405 (1982).
- ⁴ C. L. Kane and E. J. Mele, Phys. Rev. Lett. **95**, 146802 (2005).
- ⁵ L.Fu and C. L. Kane, Phys. Rev. B **76**, 045302 (2007).
- ⁶ L. Fu, Phys. Rev. Lett. **106**, 106802 (2011).
- ⁷ R.-J. Slager, A. Mesaros, V. Juricic, J. Zaanen, Nat. Phys. **9**, 98 (2013)
- ⁸ J. Kruthoff, J. de Boer, J. van Wezel, C. L. Kane, and R.-Jan Slager, Phys. Rev. X **7**, 041069 (2017)
- ⁹ Z. Song, T. Zhang, Z. Fang, and C. Fang, arXiv:1711.11049.
- ¹⁰ C. Fang, L. Fu, arXiv:1709.01929.
- ¹¹ C. Fang, Z. Song, and T. Zhang, arXiv:1711.11050.
- ¹² E. Khalaf, H. C. Po, A. Vishwanath and H. Watanabe, arXiv:1711.11589.
- ¹³ F. Zhang, C.L. Kane and E.J. Mele, Phys. Rev. Lett. **110**, 046404 (2013).
- ¹⁴ W. A. Benalcazar, B. A. Bernevig, and T. L. Hughes, 10.1126/science.aah6442.
- ¹⁵ F. Schindler, A. Cook, M. G. Vergniory, and T. Neupert, in APS March Meeting (2017).
- ¹⁶ Y. Peng, Y. Bao, and F. von Oppen, Phys. Rev. B **95**, 235143 (2017).
- ¹⁷ J. Langbehn, Y. Peng, L. Trifunovic, F. von Oppen, and P. W. Brouwer, Phys. Rev. Lett. **119**, 246401 (2017).
- ¹⁸ Z. Song, Z. Fang, and C. Fang, Phys. Rev. Lett. **119**, 246402 (2017).
- ¹⁹ W. A. Benalcazar, B. A. Bernevig, and T. L. Hughes, Phys. Rev. B **96**, 245115 (2017).
- ²⁰ F. Schindler, A. M. Cook, M. G. Vergniory, Z. Wang, S. S. P. Parkin, B. A. Bernevig, and T. Neupert, cond-mat/arXiv:1708.03636 (2017).
- ²¹ M. Lin and T. L. Hughes, cond-mat/arXiv:1708.08457.
- ²² M. Ezawa, Phys. Rev. Lett. **120**, 026801 (2018).
- ²³ M. Ezawa, arXiv:1801.00437.
- ²⁴ M. Geier, L. Trifunovic, M. Hoskam, and P. W. Brouwer, arXiv:1801.10053.
- ²⁵ E. Khalaf, arXiv:1801.10050.
- ²⁶ F. Schindler, Z. Wang, M. G. Vergniory, A. M. Cook, A. Murani, S. Sengupta, A. Y. Kasumov, R. Deblock, S. Jeon, I. Drozdov, H. Bouchiat, S. Gueron, A. Yazdani, B. A. Bernevig, and T. Neupert, arXiv:1802.02585.
- ²⁷ B. Bradlyn, L. Elcoro, J. Cano, M. G. Vergniory, Z. Wang, C. Felser, M. I. Aroyo, and B. A. Bernevig, Nature **547**, 298 (2017).
- ²⁸ M. G. Vergniory, L. Elcoro, Z. Wang, J. Cano, C. Felser, M. I. Aroyo, B. A. Bernevig, and B. Bradlyn, Phys. Rev. E **96**, 023310 (2017).
- ²⁹ L. Elcoro, B. Bradlyn, Z. Wang, M. G. Vergniory, J. Cano, C. Felser, B. A. Bernevig, D. Orobengoa, G. Flor, and M. I. Aroyo, Journal of Applied Crystallography **50** (2017).
- ³⁰ J. Cano, B. Bradlyn, Z. Wang, L. Elcoro, M. G. Vergniory, C. Felser, M. I. Aroyo, and B. A. Bernevig, cond-mat/arXiv:1709.01935
- ³¹ B. Bradlyn, L. Elcoro, M. G. Vergniory, J. Cano, Z. Wang, C. Felser, M. I. Aroyo, and B. A. Bernevig, ArXiv e-prints (2017), cond-mat/arXiv:1709.01937
- ³² J. Cano, B. Bradlyn, Z. Wang, L. Elcoro, M. G. Vergniory, C. Felser, M. I. Aroyo, and B. A. Bernevig, cond-mat/arXiv:1711.11045
- ³³ B. A. Bernevig, T. L. Hughes, and S.-C. Zhang, Science **314**, 1757 (2006).

³⁴ M. Legner, A. Ruegg, and M. Sigrist, Phys. Rev. B 89, 085110 (2014).

³⁵ M. Lin and T. L. Hughes, cond-mat/arXiv:1708.08457.